

## Article

# The Synthesis and Synergistic Effect of Heterocyclic Groups Grafted on Acrylic Polymers by Ester Groups for Marine Antifouling

Dazhuang Wang <sup>1,†</sup>, Ruotong Liu <sup>1,†</sup>, Xiaohui Liu <sup>2</sup>, Guangwen Hu <sup>1</sup>, Zhineng Fu <sup>3</sup>, Miao Dong <sup>1,4</sup> , Liju Liu <sup>1</sup>, Xinrui Lin <sup>1</sup>, Ping Zhang <sup>4</sup>, Junhua Chen <sup>1</sup>, Jianxin Yang <sup>1,4,\*</sup>  and Xinghua Xue <sup>1,\*</sup>

- <sup>1</sup> Key Laboratory of Green Catalysis and Reaction Engineering of Haikou, College of Chemistry and Chemical Engineering, Hainan University, Haikou 570228, China; 20190401310010@hainanu.edu.cn (D.W.); 20203103031@hainanu.edu.cn (R.L.); 18779689330@163.com (G.H.); dmmc2017@163.com (M.D.); liulju@163.com (L.L.); 22220856000024@hainanu.edu.cn (X.L.); klchjh@126.com (J.C.)
- <sup>2</sup> School of Food Science and Engineering, Hainan University, Haikou 570228, China; 20203100750@hainanu.edu.cn
- <sup>3</sup> College of Tropical Crops, Hainan University, Haikou 570228, China; 22210901000057@hainanu.edu.cn
- <sup>4</sup> Key Laboratory of Advanced Materials of Tropical Island Resources, Ministry of Education, Hainan University, Haikou 570228, China; zpyyh@hainanu.edu.cn
- \* Correspondence: yangjxmail@hainanu.edu.cn (J.Y.); xxh408@163.com (X.X.); Tel.: +86-136-3764-3765 (J.Y.)
- † These authors contributed equally to this work.

**Abstract:** Using a synthetic antifoulant is an alternative technique to using a natural antifoulant for its economical and large-scale production characteristics. In this study, we synthesized allyl 3-oxzo[d]isothiazole-2(3H)-carboxylate (BIT-C) and a series of other heterocyclic compounds, including triazole, pyridine, and thiazole derivatives. These heterocyclic monomers were used to prepare a new series of acrylic polymers by grafting them onto the side chains. The weight change on the 42nd day was less than  $-0.091 \text{ mg/cm}^{-2}$ , indicating that antifoulants can be released into seawater consistently and enduringly. The antibacterial and anti-algae tests revealed that all the polymers had exceptional inhibition rates on *E. coli*, *S. aureus*, *Chlorella*, and *Chaetoceros curvisetus*, with the highest inhibition rates of 99.81%, 99.22%, 92.70%, and 95.42%, respectively. Furthermore, the oyster and barnacle density and algae coverage rate were only about 200 per square meter and 10%, compared to 1800 per square meter and 100% of a blank plate after 90 days hanging in a real marine environment, showing a promising antifouling performance. This work verifies the possibility of a method for grafting different heterocycles on a single polymer to make a series of polymers that can be useful as an environmentally friendly antifouling coating.

**Keywords:** antifouling coating; heterocyclic antifoulant; antibacterial; anti-algae; marine fouling



**Citation:** Wang, D.; Liu, R.; Liu, X.; Hu, G.; Fu, Z.; Dong, M.; Liu, L.; Lin, X.; Zhang, P.; Chen, J.; et al. The Synthesis and Synergistic Effect of Heterocyclic Groups Grafted on Acrylic Polymers by Ester Groups for Marine Antifouling. *Coatings* **2023**, *13*, 1643. <https://doi.org/10.3390/coatings13091643>

Academic Editor: Thomas Lampke

Received: 28 August 2023

Revised: 13 September 2023

Accepted: 15 September 2023

Published: 19 September 2023



**Copyright:** © 2023 by the authors. Licensee MDPI, Basel, Switzerland. This article is an open access article distributed under the terms and conditions of the Creative Commons Attribution (CC BY) license (<https://creativecommons.org/licenses/by/4.0/>).

## 1. Introduction

Marine fouling is thought to be the adhesion and accumulation of undesirable micro- and macroorganisms on the surface of equipment, especially ships [1–3]. In general, the biofouling adhering to ships will increase their weight and hydrodynamic drag force, slow down their speed, and raise their fuel consumption and CO<sub>2</sub> and SO<sub>2</sub> emissions [4]. Moreover, biofouling can initiate and accelerate the corrosion of marine equipment, diminishing the service life of the equipment and causing a potential safety hazard [5,6]. It is also reported that the costs of biofouling on the Navy's entire DDG-51 class are estimated to be over 56 million USD per year, with a total cost of 1 billion USD over 15 years [7]. Despite various methods for dealing with marine fouling, the use of antifouling coatings remains the most practical and effective approach [8,9].

In previous research, tributyltin (TBT) coatings, which were widely used for restraining marine fouling in the early 1970s, were banned due to their high toxicity to animals and

the environment [10,11]. As a result, the development of highly efficient, low-toxic, and environmentally friendly coatings is receiving tremendous attention [12]. Researchers have developed six main strategies for antifouling in the past decades [13]: micro/nanostructured surfaces [14], natural or synthetic antifoulants [15,16], mucus-like hydrogels [17], slippery liquid-infused porous surfaces [18,19], dynamic surfaces [20], and zwitterionic coatings [21]. Among these strategies, coatings containing natural antifoulants are effective and environmentally friendly due to their natural and biodegradable properties. These kinds of coatings release antifoulants that can restrain biofouling [22], but the economical and massive production of these natural antifoulants, as well as a steady and long-lasting release rate, are still limits to their use [13,23–25].

Natural antifoulants have been investigated for their diversification, degradability, high efficiency, and broad spectrum against bacteria and algae. The principle of “from nature for nature” has attracted researchers to discover and examine hundreds of natural antifoulants [26]. However, their high cost and complicated extraction process hinder their widespread application. As a consequence, synthetic antifoulants, which can also be degraded in seawater, are alternative approaches used for antifouling [27–29]. Among these synthetic antifoulants, heterocyclic compounds with a considerable inhibition on bacteria, algae, and fungus have been widely investigated [30,31]. 1,2-benzisothiazol-3(2H)-one (BIT) is broadly used as an antifoulant for its low toxicity, high stability, and broad-spectrum antibacterial activity [32,33]. Furthermore, Eung Chil Choi reported that substituting a heterocyclic pyridine with bactericidal characteristics onto oxazolidinone can improve its efficacies against relevant resistant Gram-positive organisms [34]. Feng Gao reported several heteroaromatic ring 1,2,4-triazoles that have the same properties as first-line antibacterial agents [35]. Samir Y. Abbas and Yousry A. Ammar reported that the thiazole moiety in quinolines can be developed into antibacterial and antifungal compounds [36]. Hence, BIT derivatives, as well as other triazole, pyridine, and thiazole derivatives with a high efficiency in inhibiting bacteria and algae, can be synthesized for marine antifouling.

The limitations of economically and massively producing natural antifoulants can be resolved through alternative methods, while a steady and long-lasting release rate can be effectively managed through the use of polymeric coatings with antifoulants grafted on their side chains. In this method, the antifoulants can be hydrolyzed and released into seawater gradually, while controlling the release rate via various conjugation methods and antifoulant contents [37,38].

Among the available polymeric coatings, the acrylic polymer is one of the most widely used polymers because of its favorable film-forming properties and excellent self-polishing performance [28,39,40]. Moreover, research on acrylic resin has been conducted since the 1960s. Dong et al. conducted a study that demonstrated acrylic resin’s potential as a matrix material for the preparation of GO nanocomposites [41]. Additionally, acrylic resins have been explored for their use as dental restorative materials in the field of medicine [42]. Furthermore, the waterborne acrylic resin exhibits environmentally friendly, health-conscious, and safe characteristics, which make it a promising option for waterproof and anticorrosive coatings [43]. Therefore, controlling the release rate of antifoulants is possible by changing the content of these antifoulants and designing the side chain structures of the acrylic polymer.

In this work, an allyl ester group was introduced to BIT and other heterocyclic compounds, including triazole, pyridine, and thiazole, via substitution reactions. These heterocyclic compounds have similar structures to bactericide, can also have a bactericidal effect, and possess an antifouling ability [32,34–36]. Subsequently, a series of novel acrylic polymers were synthesized using the random free radical polymerization of BIT monomer, heterocyclic monomer, methyl methacrylate (MMA), and butyl acrylate (BA). A schematic illustration of the marine antifouling mechanism of the polymers containing antifoulants is shown in Figure 1. The BIT and heterocyclic compounds were grafted onto the side chains of acrylic polymers through the ester group that could hydrolyze steadily in seawater.

ter. Thus, the acrylic polymer could release the effective antifoulants in a controlled and long-lasting way to prevent marine fouling from adhering. In addition, the results demonstrated that the acrylic polymers containing both BIT and heterocyclic groups, especially thiazole monomers, exhibited superior antibacterial, anti-algal properties, and antifouling performances, implying that allyl 3-oxobenzo[d]-iso-thiazole-2(3H)-carboxylate (BIT-C) and other heterocyclic groups can have a synergistic inhibition effect on marine antifouling.

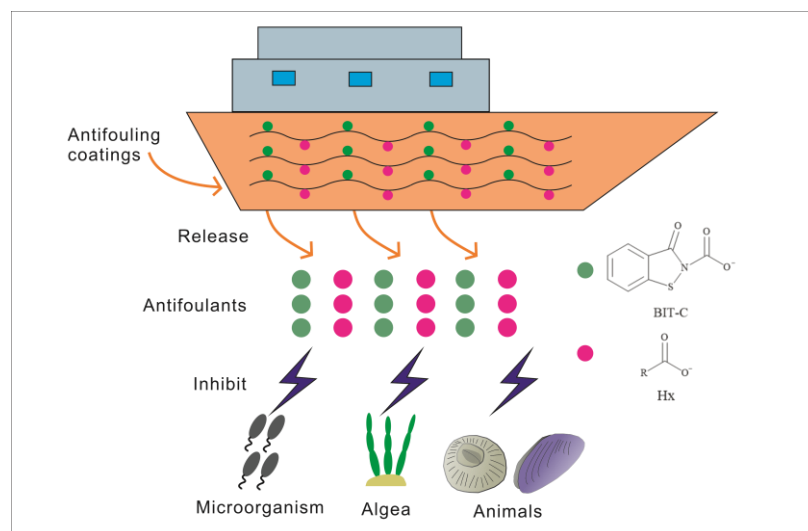


**Figure 1.** Schematic illustration of the marine antifouling mechanism of the polymers containing antifoulants.

## 2. Materials and Methods

### 2.1. Materials

1,2-Benzisothiazolin-3-One (BIT), methylbenzene, allyl chloroformate, triethylamine, anhydrous magnesium, 3-mercapto-1,2,4-triazole, xylene, n-butanol, Methyl methacrylate (MMA), butyl acrylate (BA), and 2,2'-Azobis(2-methylpropionitrile) (AIBN) were purchased from Aladdin without further purification.

### 2.2. Synthesis of Allyl 3-Oxobenzo[d]isothiazole-2(3H)-carboxylate (BIT-C)

The reaction of BIT (1.51 g, 0.010 mol) with methylbenzene (45 mL) and allyl chloroformate (1.44 g, 0.012 mol) in the presence of triethylamine (4 drops) in a 100 mL round-bottom flask was stirred with a magnetic bar, and then refluxed for 5 h. After that, the pH of the reaction mixture was neutralized with a sodium hydroxide solution and washed with deionized water three times. The organic layer was separated and dried over anhydrous magnesium sulfate. The organic layer was then evaporated under reduced pressure to obtain allyl 3-oxobenzo[d]isothiazole-2(3H)-carboxylate (BIT-C) as a solid product.

BIT-C: white solid powder with a yield of 82.5%,  $^1\text{H}$  NMR (400 MHz,  $\text{DMSO-}d_6$ ),  $\delta$  8.09 (d, 1H, PhH), 7.73 (t, 1H, PhH), 7.53 (d, 1H, PhH), 7.44 (t, 1H, PhH), 6.12–6.02 (m, 1H,  $-\text{CH}=\text{}$ ), 5.58–5.53 (d, 1H,  $=\text{CH}_2$ ), 5.42–5.38 (d, 1H,  $=\text{CH}_2$ ), and 4.94 (d, 2H,  $\text{CH}_2$ ).

### 2.3. Synthesis of Heterocyclic Monomers (Hx)

All heterocyclic monomers can be synthesized using the reaction of various heterocyclic compounds with allyl chloroformate to introduce a carbon–carbon double bond for polymerization. For instance, 3-mercapto-1,2,4-triazole (0.010 mol), methylbenzene (45 mL), and triethylamine (0.012 mol), were added to a 100 mL round-bottom flask equipped with a reflux condenser. The mixture was stirred and heated to 60 °C, and then allyl chloroformate (0.012 mol) was added dropwise. After the completion of the addition, the reaction mixture was refluxed for 4–6 h. After that, the reaction mixture was washed with deionized water three times, and the organic layer was evaporated under reduced pressure to obtain the

final product. To simplify the description, the heterocyclic monomers were named H1, H2, H3, H4, H5, H6, and H7, respectively. The  $^1\text{H}$  NMR of H1–H7 are as follows:

H1: O-allyl S-(1H-1,2,4-triazol-3-yl) carbonothionate.  $^1\text{H}$  NMR (400 MHz,  $\text{DMSO-}d_6$ ),  $\delta$  14.05 (s, 1H, NH), 8.45 (s, 1H, N=CH), 5.98–5.87 (m, 1H, =CH<sub>2</sub>), 5.25–5.20 (d, 1H, =CH<sub>2</sub>), 5.07–5.03 (d, 1H, =CH<sub>2</sub>), and 3.76 (d, 2H, CH<sub>2</sub>).

H2: Allyl pyridin-2-ylcarbamate.  $^1\text{H}$  NMR (400 MHz,  $\text{DMSO-}d_6$ ),  $\delta$  10.25 (s, 1H, NH), 8.28 (d, 1H, PhH), 7.84 (d, 1H, PhH), 7.80–7.75 (t, 1H, PhH), 7.06 (t, 1H, PhH), 6.03–5.94 (m, 1H, -CH=), 5.42–5.36 (d, 1H, =CH<sub>2</sub>), 5.27–5.23 (d, 1H, =CH<sub>2</sub>), and 4.64 (d, 2H, CH<sub>2</sub>).

H3: Allyl (3-methylpyridin-2-yl) carbamate.  $^1\text{H}$  NMR (400 MHz,  $\text{DMSO-}d_6$ ),  $\delta$  9.54 (s, 1H, NH), 8.22 (d, 1H, PhH), 7.65 (d, 1H, PhH), 7.16 (m, 1H, PhH), 6.01–5.92 (m, 1H, -CH=), 5.37–5.33 (d, 1H, =CH<sub>2</sub>), 5.23–5.20 (d, 1H, =CH<sub>2</sub>), 4.58 (d, 2H, CH<sub>2</sub>), and 2.20 (s, 3H, CH<sub>3</sub>).

H4: Allyl (5-methylpyridin-2-yl) carbamate.  $^1\text{H}$  NMR (400 MHz,  $\text{DMSO-}d_6$ ),  $\delta$  10.11 (s, 1H, NH), 8.16 (s, 1H, PhH), 7.73 (d, 1H, PhH), 7.60 (d, 1H, PhH), 6.03–5.93 (m, 1H, -CH=), 5.41–5.35 (d, 1H, =CH<sub>2</sub>), 5.26–5.22 (d, 1H, =CH<sub>2</sub>), 4.62 (d, 2H, CH<sub>2</sub>), and 2.24 (s, 3H, CH<sub>3</sub>).

H5: Allyl thiazol-2-ylcarbamate.  $^1\text{H}$  NMR (400 MHz,  $\text{DMSO-}d_6$ ),  $\delta$  11.82 (s, 1H, NH), 7.40 (d, 1H, PhH), 7.20 (d, 1H, PhH), 6.04–5.94 (m, 1H, -CH=), 5.42–5.36 (d, 1H, =CH<sub>2</sub>), 5.29–5.25 (d, 1H, =CH<sub>2</sub>), and 4.70 (d, 2H, CH<sub>2</sub>).

H6: Allyl benzo[d]thiazol-2-ylcarbamate.  $^1\text{H}$  NMR (400 MHz,  $\text{DMSO-}d_6$ ),  $\delta$  12.15 (s, 1H, NH), 7.97 (d, 1H, PhH), 7.71 (d, 1H, PhH), 7.43 (t, 1H, PhH), 7.30 (t, 1H, PhH), 6.07–5.97 (m, 1H, -CH=), 5.45–5.40 (d, 1H, =CH<sub>2</sub>), 5.32–5.28 (d, 1H, =CH<sub>2</sub>), and 4.75 (d, 2H, CH<sub>2</sub>).

H7: Allyl (6-methylbenzo[d]thiazol-2-yl) carbamate.  $^1\text{H}$  NMR (400 MHz,  $\text{DMSO-}d_6$ ),  $\delta$  12.06 (s, 1H, NH), 7.76 (s, 1H, PhH), 7.59 (d, 1H, PhH), 7.24 (d, 1H, PhH), 6.06–5.96 (m, 1H, -CH=), 5.44–5.39 (d, 1H, =CH<sub>2</sub>), 5.31–5.28 (d, 1H, =CH<sub>2</sub>), 4.73 (d, 2H, CH<sub>2</sub>), and 2.41 (s, 1H, CH<sub>3</sub>).

#### 2.4. Synthesis of Polymer APBHx

The typical procedure for the synthesis of APBH1, BIT-C (4.0 g), and O-allyl S-(1H-1,2,4-triazol-3-yl) carbonothionate (H1) (4.0 g) is to dissolve them in a mixture solvent of xylene and n-butanol (4:1) in a round-bottom flask equipped with a reflux condenser and a magnetic stirring bar. MMA (6.0 g) and BA (6.0 g) were also employed in the reaction mixture to obtain the mechanical properties of the polymer. After dissolving all the monomers, AIBN (0.92 g) was added as the radical polymerization initiator and the reaction was refluxed at 80–90 °C under a nitrogen atmosphere for 5–9 h. After the reflux, the final polymer was allowed to cool and was named APBH1. In the same way, all the polymers were prepared by using different heterocyclic monomers and named as APBHx, where x is the number of heterocyclic monomers. The synthetic routes and chemical structures of the monomers and polymers are presented in Scheme 1.

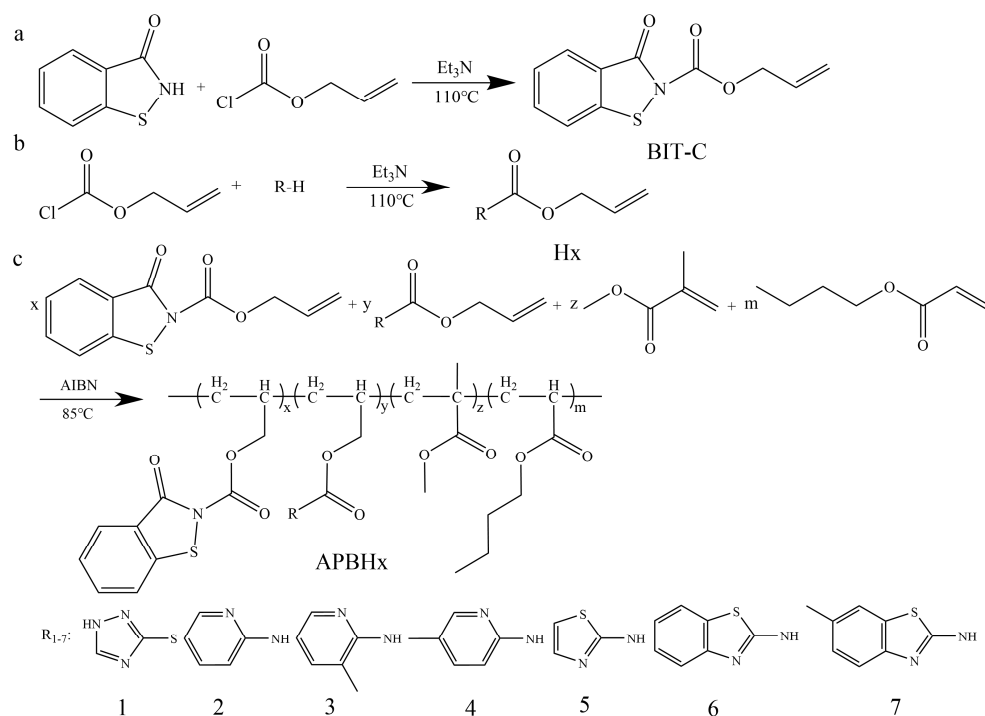
#### 2.5. Characterization

Proton Nuclear Magnetic Resonance Spectroscopy ( $^1\text{H}$  NMR):  $^1\text{H}$  NMR (400 MHz) was recorded on a Bruker AVANCE instrument (BRUKER av-400, Nasdaq: BRKR, Romanshorn, Switzerland), using  $\text{DMSO-}d_6$  as the solvent at room temperature under 400 MHz, with TMS as the internal standard.

Fourier transform infrared spectra (FTIR): An FTIR analysis of the polymers was carried out on a Bruker TENSOR 27 FTIR spectrometer (Thermo Fisher Scientific, Waltham, MA, USA) by applying the polymers onto potassium bromide flakes, with the wavelength range from 4000 to 400  $\text{cm}^{-1}$  and scanning 32 times. The test temperature was room temperature.

Gel Permeation Chromatography (GPC). The instrument model was Waters 1515 (Waters Co, Milford, MA, USA), equipped with a refractive index detector (Waters 2414), syringe (Waters 717), HPLC pump (Waters 515), and three Styragel columns (particle size: 10 micron). In total, 0.05 g of polymer dissolved in 1 mL of tetrahydrofuran (THF) was weighed to a concentration of approximately 5 mg/mL for determination. Using

tetrahydrofuran as the mobile phase, the column temperature was 35 °C with a flow rate of 1 mL/min. The calibration curve was confirmed with the polystyrene (PS) standard.



**Scheme 1.** Synthetic routes of (a) BIT monomer, (b) heterocyclic monomers, and (c) heterocyclic acrylate polymers.

## 2.6. Thermal Analysis

**Thermogravimetric Analysis (TGA):** A thermogravimetric analysis of the polymers was conducted on a Q600 SDT (TA Inc., New Castle, DE, USA) thermogravimetric analyser, with a temperature range of 20–600 °C and a heating rate of 10 min/°C under a nitrogen atmosphere. About 5–10 mg of polymers was placed in an alumina crucible for the TGA test.

## 2.7. Weight Change Measurement

The weight change of the polymers was measured using boiled sea water. About 3.0 g of polymers was brushed onto the glass plates (75 × 25 × 1.2 mm) and dried to a constant weight at room temperature, then put into the bakers with boiled sea water and stirred at the same frequency. The weights of the plates were recorded every 7 days after the plates were taken out, rinsed with deionized water, and dried to a constant weight at room temperature. In consideration of fact that the polymer would absorb sea water, which would make the weight higher than the initial weight, we used the  $\Delta W$  (mg/day) to explain the water absorption and hydrolysis of the polymers. The  $\Delta W$  was calculated as follows:

$$\Delta W = W_{t+1} - W_t \quad (1)$$

$W_t$  represents the weight on day  $t$  and  $W_{t+1}$  represents the weight on day  $t + 1$ . The reported  $\Delta W$  was the average of three parallel measurements.

## 2.8. Water Contact Angle Test

The water contact angle (WCA) of the polymers was measured on the Optical Surface Analyzer 60. The polymers were brushed onto glass plates (75 × 25 × 1.2 mm) and dried at room temperature, then 5.0  $\mu\text{L}$  of deionized water was dropped onto the plate for the WCA test. The result of the WCA test was an average of five measurements taken at random positions on the same plate. The WCA of the polymers immersed in boiled sea water for 7

days was also measured to understand the surface structure changes in the polymers after hydrolysis.

### 2.9. Antibacterial Test

Gram-negative bacteria, namely *Escherichia coli* (*E. coli*), and Gram-positive bacteria *Staphylococcus aureus* (*S. aureus*) were chosen for the antibacterial test [41,42]. About 2 mL of polymers was coated onto the cell culture plates and dried naturally. Then, *E. coli* and *S. aureus* were cultured using tryptone soybean broth (TSB) as the culture solution. With an initial optical density (OD) of about 0.02, 60  $\mu$ L of bacteria and 3 mL of liquid culture solution were added into the cell plates and cultured at 37 °C in an incubator. The absorbance of the bacteria was recorded using a UV-vis spectrophotometer at 600 nm after 12 h, 24 h, 36 h, and 48 h, respectively. The bacterial inhibition rate ( $I_b$ ) can be calculated using the absorption according to the following equation:

$$I_b = (A_{b0} - A_{bi}) / (A_{b0} - A_{bp}) \quad (2)$$

where  $I_b$  is the bacterial inhibition rate,  $A_{b0}$  is the absorption of the bacteria without the polymers coated,  $A_{bi}$  is the absorption of the bacteria with the polymers coated, and  $A_{bp}$  is the absorption of the cell plates. The reported  $I_b$  was the average of three parallel measurements.

### 2.10. Anti-Algae Test

*Chlorella* and *Chaetoceros curvisetus* were chosen for the anti-algae test. The maximum absorption wavelengths of *Chlorella* and *Chaetoceros curvisetus* were determined on a UV-vis spectrophotometer (TU-1901, Beijing Purkinje GENERAL Instrument Co., Ltd., Beijing, China) and were 690 and 690 nm, respectively. The algae solution was then diluted to reduce the absorption to about 0.05 Abs. After that, the polymers were brushed onto glass plates (75  $\times$  25  $\times$  1.2 mm), dried at room temperature, and immersed in 200 mL of the algae solution. The absorptions of the algae solutions were measured every 24 h for 7 days, with a blank plate serving as the control group. As the absorbance of the algae solutions was directly proportional to their concentration, the algae inhibition rate ( $I_a$ ) can be calculated using the absorption of an algal solution according to the following equation:

$$I_a = (A_0 - A_i) / A_0 \quad (3)$$

where  $I_a$  is the algae inhibition rate,  $A_0$  is the absorption of the algae solution with the blank plate, and  $A_i$  is the absorption of the algae solution with the polymer-coated plate. The reported  $I_a$  was the average of three parallel measurements.

### 2.11. Marine Field Test

The marine field test was conducted in the South China Sea (110°19' E, 20°1' N) from November to February. The sea contains sponges, algae, barnacles, mussels, lime worms, and bryozoans, with temperatures ranging from 22 to 28 °C. Epoxy resin plates (200  $\times$  300 mm) were first wiped with ethanol and deionized water, then used as the substrates for the polymers. After the polymers were coated onto the plates and dried at room temperature, a blank plate was used as the control group. The marked epoxy resin plates were then immersed in marine water at a depth of 1–2 m below sea level. The plates were taken out every 30 days, the sludge was cleaned with seawater, and the plates were photographed and put back immediately for further marine field tests. The test was conducted once but was reliable due to the long test time.

## 3. Results and Discussion

### 3.1. Characterization

The indication of the polymerization determined using GPC is shown in Table 1. The observed ranges for the number-averaged molecular weights ( $M_n$ ) and weight-averaged molecular weights ( $M_w$ ) of the polymers were from 4348 to 9727 and from 6401 to 26,465,

respectively. APBH1 and APBH7 had smaller  $M_n$  and  $M_w$  values than the rest, indicating a lower polymerization. We think this is because the O-allyl S-(1H-1,2,4-triazol-3-yl) carbonothionate was less active compared to the other heterocyclic monomers, and a larger steric hindrance in allyl (6-methylbenzo[d]thiazol-2-yl) carbamate blocked its polymerization. The poly dispersity indexes (PDIs) ranged between 1.47 and 2.72, implying a goodish weight distribution.

**Table 1.** Composition and molecular weight of APBHx.

Samples	Weight Ratio of Monomer (%)	$M_n$ (g mol <sup>-1</sup> )	$M_w$ (g mol <sup>-1</sup> )	PDI
	MMA/BA/Hx/BIT-C			
APBH0	40/40/0/20	5894	13,339	2.26
APBH1	30/30/20/20	4348	6401	1.47
APBH2	30/30/20/20	8318	19,849	2.39
APBH3	30/30/20/20	8640	22,200	2.57
APBH4	30/30/20/20	9727	26,465	2.72
APBH5	30/30/20/20	6619	12,429	1.88
APBH6	30/30/20/20	6741	14,607	2.16
APBH7	30/30/20/20	5044	9005	1.79

APBH7 was selected as a representative sample to determine whether the synthesis was successful in the <sup>1</sup>H NMR spectrum (Figure 2a). In Figure 2a, the small multiple peaks at  $\delta = 8.4$ –7.4 (a) indicate the presence of benzene rings, and the characteristic peaks of OCH<sub>2</sub> can be observed at  $\delta = 5.1$  (b). Additionally, the peaks at  $\delta = 4.0$ –3.4, which correspond to the RCOOCH<sub>3</sub> or RCOOCHR, can be observed at  $\delta = 4.0$  (c) and  $\delta = 3.6$  (d). According to the above analysis, it can be confirmed that the BIT monomer, heterocyclic monomer, MMA, and BA were grafted onto the polymer chain. Therefore, not only could the structure of APBH7 be determined, but it was also determined that all the functional monomers were involved in the polymerization.

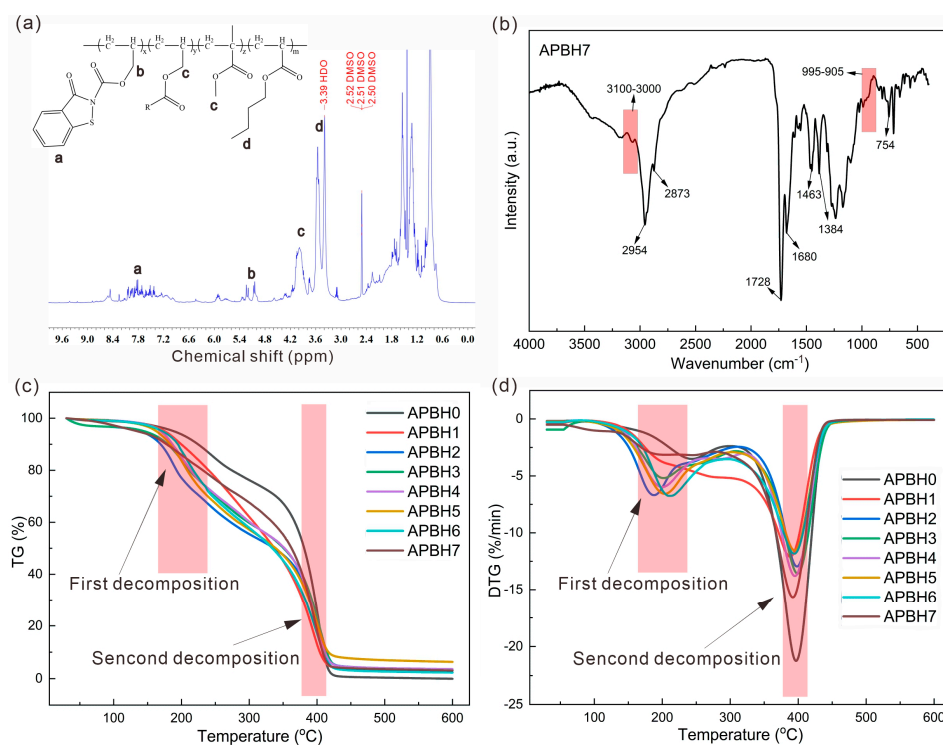


**Figure 2.** Characterization and thermal analysis of the polymers. (a) <sup>1</sup>H NMR of APBH7, (b) FTIR of APBH7 (c) TGA, and (d) DTG curves of APBHx.

The FTIR of APBH7 is shown in Figure 2b. It is noticeable that there were no evident peaks at 3100–3000 and 995–905  $\text{cm}^{-1}$  (red frame), which are characteristic peaks of carbon–carbon double bonds. Therefore, it is proven that the process of free radical polymerization was complete. Moreover, there were characteristic peaks of the methyl group observed at 2954, 2873, and 1384  $\text{cm}^{-1}$ , while the ester and amide groups had strong characteristic peaks at 1728 and 1680  $\text{cm}^{-1}$  that are also observed in Figure 2b. The presence of multiple absorption peaks at 1463  $\text{cm}^{-1}$  indicated the presence of a benzene ring, while the presence of peaks at 754  $\text{cm}^{-1}$  implied that the benzene was an ortho-disubstituted benzene. Therefore, the FTIR analysis of APBH7 revealed all the functional groups, and the absence of a carbon–carbon double bond indicated that the polymers were synthesized successfully.

### 3.2. Thermal Analysis

The volatile content, decomposition temperature ( $T_d$ ), and thermal stability of the polymers determined using TGA is shown in Figure 2c. It is observed that the APBH0, which only contained the BIT monomer, began to decompose at 200  $^{\circ}\text{C}$ , while APBH1–APBH7 began to decompose at 150  $^{\circ}\text{C}$ , showing a lower start  $T_d$ . This can be attributed to the lower decomposition of the heterocyclic monomers. When the temperature was above 450  $^{\circ}\text{C}$ , all of APBHx was decomposed completely, which is in accordance with other general acrylic polymers [10,44,45].

The derivative thermogravimetry (DTG) curves exhibiting the weight loss rate of APBHx are shown in Figure 2d. It can be easily concluded that there were two steps in the decomposition of APBHx during the temperature increase. The first step, with a smaller weight loss, occurred at 150–250  $^{\circ}\text{C}$ , corresponding to residual solvent, small molecular polymers, and some heterocyclic side chains. The second step, with the main weight loss, occurred at 300–450  $^{\circ}\text{C}$ . In this step, the main chain of the polymers decomposed, resulting in the production of alcohol, methanal, and carbon dioxide, etc. Therefore, the polymers decomposed at 150–450  $^{\circ}\text{C}$ , while a lower initial decomposition temperature and higher weight loss were exhibited at 150–250  $^{\circ}\text{C}$  when the other heterocyclic monomers were introduced.

### 3.3. Weight Change Measurements

The weight change was measured to understand the water absorption and hydrolysis rate of the polymers (Figure 3a). During the first 0 to 14 days, the weight of most polymers increased, implying that the seawater absorption was faster than the hydrolysis at the beginning. It is noteworthy that the polymers grafted with heterocyclic monomers showed a lower weight increase due to their higher hydrolysis rate and hydrophobicity. When the plates were immersed for 21 to 42 days, the weight of polymers decreased and inclined in terms of stabilization at the end, because the hydrolysis rate became higher than the water absorption rate, since the polymers had already absorbed a considerable amount of water. On the 42nd day, the weight change was between  $-0.091 \text{ mg}/\text{cm}^{-2} \text{ d}$  and  $0.011 \text{ mg}/\text{cm}^{-2} \text{ d}$ , which meant the antifoulants could be released in a control rate.

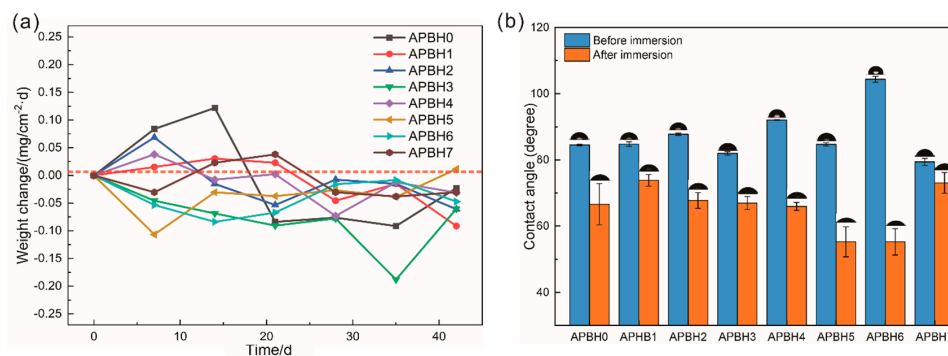


**Figure 3.** Hydrolysis and wettability of APBHx. (a) Weight changes in APBHx during immersion in seawater for 42 days, and (b) WAC of APBHx before immersion and after immersion in seawater for 7 days. The error bars represent the standard deviation.

### 3.4. Water Contact Angle Test

The wettability and surface structure changes before and after the hydrolysis of the polymers were investigated by measuring the WCA before and after immersion for 7 days (Figure 3b). It can be observed that the WCA of the polymers was between  $79.39^\circ$  and  $104.36^\circ$  before immersion. It is worth mentioning that the APBH4 and APBH6 showed hydrophobicity due to their WCA being above  $90^\circ$ , while the rest of the polymers were hydrophilic. This also corresponded to the weight increase observed in the weight change measurements, because the polymers could absorb seawater due to their wettability.

Moreover, the WCA of the polymers after immersion was significantly lower than the WCA before immersion, ranging from  $55.27^\circ$  to  $73.86^\circ$ . This was because of the hydrolysis process, which released hydrophobic groups such as heterocyclic groups and butyl groups into the seawater, while transferring hydrophilic groups such as  $-\text{COO}-$  to the surface. It is worth noting that the error bars were significantly larger after immersion, indicating that all the polymers were hydrolyzed unevenly.

### 3.5. Antibacterial Test

The antibacterial activity of the polymers was probed by testing the absorbance of bacteria at 600 nm (Figure 4a,b). The inhibition rate on *E. coli* was between 87.57% and 99.81%, showing excellent antibacterial activity. The inhibition rate only had a slight decrease with the extension of time, which meant the polymers could effectively inhibit the growth of *E. coli*. Notably, the inhibition rates of APBH2 and APBH3 were lower than those of the other polymers, implying that some heterocyclic compounds had antagonistic effects. The inhibition rate of *S. aureus* increased as the time did, with a high inhibition rate range from 98.13% and 99.22%. That meant the polymers had effective antibacterial activity on *S. aureus*. Thus, it can be concluded that the polymers had brilliant antibacterial activity, and incorporating a pyridine ring may have had an antagonistic effect with BIT on the inhibition of *E. coli*.

### 3.6. Anti-Algae Test

*Chlorella* and *Chaetoceros curvisetus* were selected to investigate the anti-algae abilities of the polymers, as *Chlorella* has a rapid growth rate and *Chaetoceros curvisetus* is a common diatom in marine environments. The inhibition of the polymers on the algae and images of the algae solutions on the 7th day are shown in Figure 4e,f.

APBHx inhibited the growth of *Chlorella*, as shown in Figure 4c. It is noticeable that, except from with APBH6, the absorbance of the *Chlorella* solution increased during the first two days, indicating that the algae were growing normally. This was because the antifoulants had not been released yet and could not inhibit the growth efficiently. In addition, the absorbance of APBH6 decreased by 0.012 Abs on the second day compared to the first day, indicating its fast anti-algae efficiency. On the last 4 days, the absorbance of the control group rose quickly, showing a good growth, while the absorbance of the *Chlorella* solution containing the polymers decreased and levelled off, suggesting that all the algae were inhibited and dying gradually.

On the 7th day, APBH0 and APBH1 had the highest *Chlorella* inhibition rate, which was 92.70%, while APBH7 had the lowest *Chlorella* inhibition rate, which was 83.21%. In conclusion, APBHx showed good inhibition against *Chlorella* growth, with an inhibition rate ranging from 83.21% to 92.70%.

APBHx inhibiting the growth of *Chaetoceros curvisetus* is shown in Figure 5. It can be observed that, at the beginning of 2 days, most of the absorbance of the *Chaetoceros curvisetus* solution decreased, apart from with APBH0 and APBH4, indicating that most of APBHx could inhibit the growth of *Chaetoceros curvisetus* on the second day. Notably, the absorbance of APBH6 decreased on the first day, revealing a quick anti-algae ability. In the last 5 days, the absorbance of the control group *Chaetoceros curvisetus* solution increased fast, while the absorbance of APBHx decreased gradually and stabilized as the antifoulants were released. This shows an efficient inhibition ability against *Chaetoceros curvisetus*.

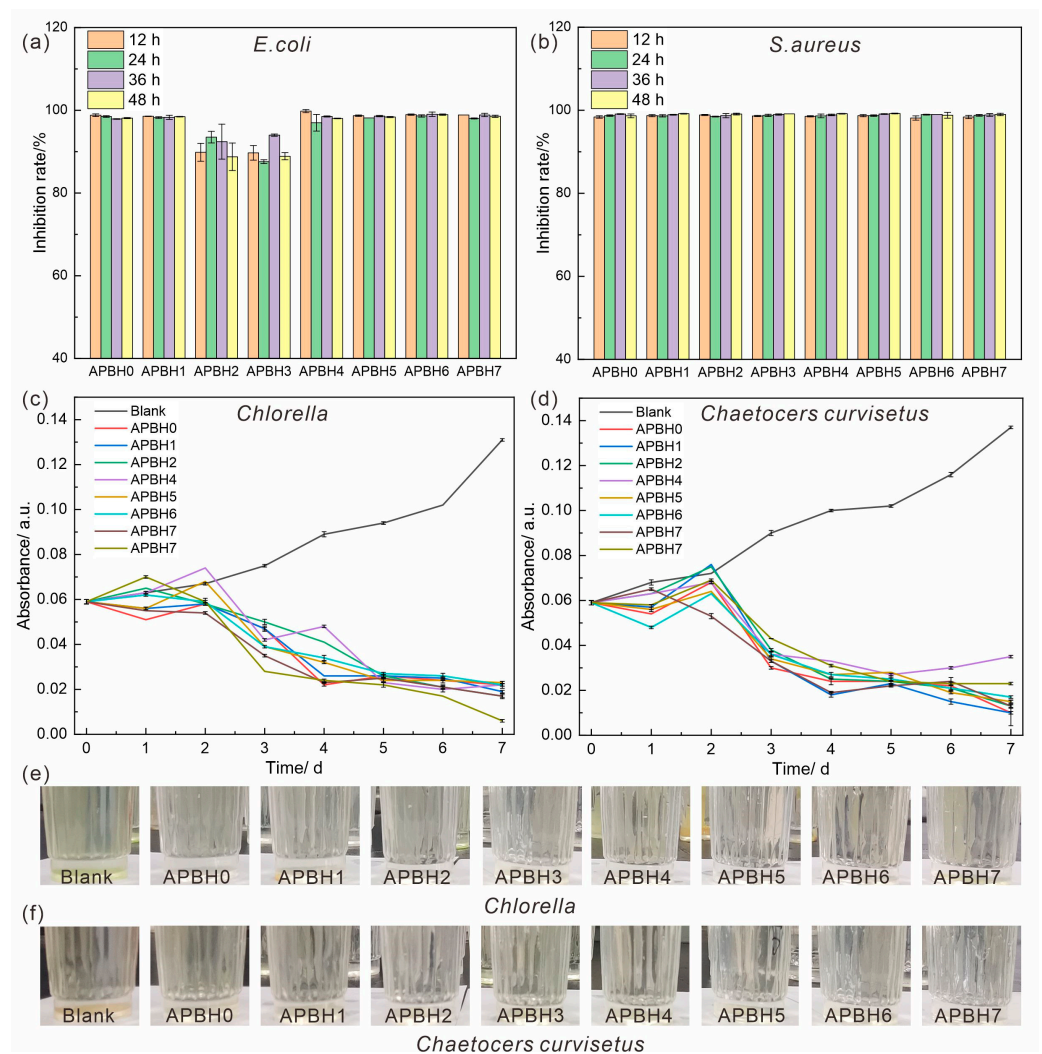


**Figure 4.** Inhibition of APBHx on algae and bacterium. (a) Inhibition rate of APBHx on *E. coli*, (b) inhibition rate of APBHx on *S. aureus*, (c) inhibition rate of APBHx on *Chlorella*, (d) inhibition rate of APBHx on *Chaetoceros curvisetus*, (e) images of *Chlorella* solutions on the 7th day, and (f) images of *Chaetoceros curvisetus* solutions on the 7th day.

On the 7th day, the inhibition rate of APBHx against *Chaetoceros curvisetus* was between 82.44% and 95.42%, indicating that *Chaetoceros curvisetus* was effectively inhibited. Among the polymers, APBH4 exhibited the lowest *Chaetoceros curvisetus* inhibition rate, which was 82.44%, while APBH7 exhibited the highest inhibition rate, which was 95.42%.

Overall, the results of the anti-algae test showed that the APBHx exhibited excellent inhibitory activities against *Chlorella* and *Chaetoceros curvisetus*, with inhibition rates ranging from 83.21% to 92.70% and from 82.44% to 95.42%, respectively. In particular, APBH6 exhibited a quick anti-algal ability, inhibiting the growth effectively on the first or second day. The current polymer coatings contain biotoxic heavy metals such as copper and tin. In contrast, the acrylic resin antifouling coating investigated in this work was characterized as green and non-toxic, making it a more favorable alternative to the existing polymer coatings. Compared with our previous work [44], this work showed similar antifouling results, indicating that the polymers we synthesized could also effectively inhibit the growth of bacterial and algae and be used as new coatings for antifouling.

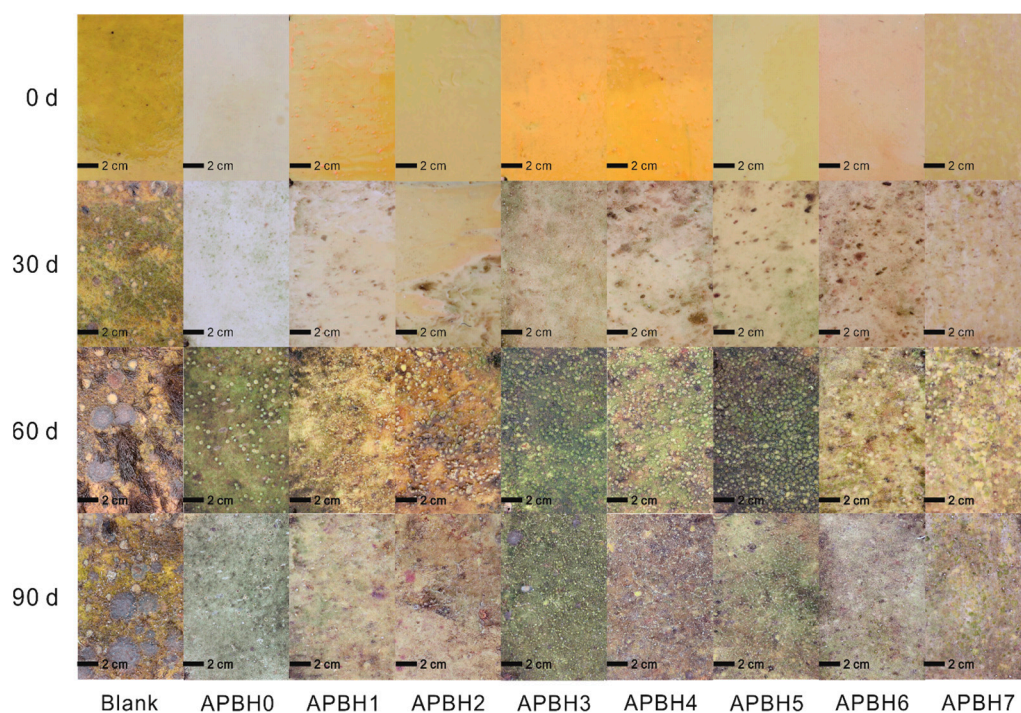


**Figure 5.** Antifouling performance of APBHx in marine field test.

### 3.7. Marine Field Test

The marine field test was conducted to investigate the real marine antifouling performance. Since the real marine environment is complicated and changeable, a marine field test is necessary to evaluate the application prospects of antifouling polymers. Photographs of the plates immersed in the marine environment for 30, 60, and 90 days are shown in Figure 5.

The hanging site was in Haikou Bay (20.0313° N, 110.3020° E), Haikou city, Hainan Province, and the surface water temperature range was 25–28 °C. The test site has a wide variety of marine detest organisms, including bacteria, algae, lime worms, bryozoans, mussels, and barnacles. The experiments were performed according to the national standard GB5370-2007. Specific steps: the epoxy resin plate coated with samples (300 × 200 × 3 mm<sup>3</sup>) was cleaned with pure water and ethanol, the series of antifouling resin coatings prepared in this study were brushed on the surface of the epoxy resin plate twice, then the coating was naturally dried and cured in a well-ventilated place, fixed onto the stainless steel frame, and immersed in seawater with a depth of 0.5–1.0 m. A blank sample (acrylic resin) was used as the control group. The hanging board time lasted for 3 months from November to January. Every month later, the epoxy plate was removed from the sea, carefully washed with seawater to remove the debris and take photographs, and immediately released back to the seawater for continued testing.

After 30 days of immersion, there were algae and barnacle larvae adhering to the blank plate, whereas little biofilm was accumulated on the APBH0-APBH7 plates, showing a good performance in inhibiting the growth of algae. After 60 days, a large number of oysters, mussels, barnacles, and algae were adhered to the blank plate, while only a small number of algae were accumulated on the APBH0, APBH3, APBH4, and APBH5 plates. Notably, the algae fell off and formed a clean circular shape on APBHx, which we attributed to two reasons: (1) The marine organisms adhering to the surface were killed or degraded by the antifoulants, then naturally fell off through the force of water flow. (2) The acrylic polymer could hydrolyze and release side chains from the surface, causing the fouling to fall off, which is similar to a self-polishing effect.

After 90 days, the blank plate had plenty of oysters, barnacles, and other hazardous macroorganisms adhered to its surface, while the APBH1, APBH2, APBH6, and APBH7

plates had only some algae and bryozoan larvae accumulated. The absence of macroorganisms on the APBH0-APBH7 plates indicated that the APBH0-APBH7 plates had good antifouling performances and were still effective after being immersed in the real marine environment for 90 days. Notably, APBH1, APBH2, APBH6, and APBH7 had a few organisms accumulated on their surfaces, exhibiting a promising application in real marine antifouling.

To analyze the antifouling effect of the polymers, we measured the density and algae coverage rate of the plates after 30, 60, and 90 days. Table 2 shows that, after 30 days, the blank plate had a growth number of 719 oysters and barnacles per square meter, while the APBH0-APBH7 plates had a growth number of 0 oysters and barnacles per square meter, indicating the effective inhibition of their attachment. The APBH1-APBH7 plates maintained a 0% coverage rate of brown algae and green algae after 30 days, compared to 57% for the blank plate and 14% for the APBH0 plate, demonstrating their excellent algae suppression effect.

**Table 2.** Density of oysters and barnacles and algae coverage rate on each sample.

Samples	Oysters and Barnacle Density (per Square Meter)			Brown Algae and Green Algae Coverage Rate (%)		
	30 Days	60 Days	90 Days	30 Days	60 Days	90 Days
Blank	719	864	1801	57	84	100
APBH0	0	558	823	14	77	100
APBH1	0	0	61	0	8	16
APBH2	0	217	355	0	7	7
APBH3	0	220	370	0	75	70
APBH4	0	283	300	0	22	14
APBH5	0	280	368	0	60	32
APBH6	0	0	48	0	11	15
APBH7	0	0	47	0	10	15

After 60 days, the density of oysters and barnacles reached 864 per square meter, and the coverage of algae was as high as 84%. On the APBH0 plate, there were 558 oysters and barnacles per square meter, with an algae coverage rate of 77%, while the APBH1-APBH7 plates had a minimal attachment of green algae. It is noteworthy that the APBH1, APBH6, and APBH7 plates had fewer than 100 oysters and barnacles per square meter, indicating their effective ability to inhibit biological attachment.

After 90 days, the density of oysters and barnacles on the blank plate was 1801 per square meter, while the number on the APBH7 plate was only 47 per square meter. This effectively demonstrated the superior antifouling performance of the polymer containing allyl (6-methylbenzo [d]) thiazol-2-yl carbamate and BIT compared to the polymer only containing BIT. Additionally, the algae coverage rate on the blank plate and APBH0 plate reached 100%, whereas the algae coverage rate of the APBH2 plate was only 7%. These findings indicate that allyl pyridin-2-ylcarbamate and BIT exhibit the best algae suppression performances.

The marine field test conducted in the marine field revealed that BIT, when cografted with other heterocyclic compounds, exhibited an excellent synergistic antifouling effect. It effectively prevented the attachment of marine fouling over an extended period and holds promising potential for marine antifouling applications.

#### 4. Conclusions

In this work, eight novel acrylic polymers, with BIT and other heterocyclic groups grafted on the side chains with ester groups, were synthesized by using free radical polymerization. The polymers demonstrated favorable and stable antifoulant release rates that could prolong the life span of the polymers in weight change measurements. Additionally, the polymers also exhibited clear and efficient inhibitory activity against

bacteria and algae. The marine field test determined that the APBH1, APBH2, APBH6, and APBH7 plates had extraordinary antifouling performances for 90 days. It can be concluded that BIT has a great synergistic effect with some heterocyclic groups such as triazole and benzothiazole derivatives, showing higher inhibitory activity and a better antifouling performance than the original polymer. Consequently, the polymers we synthesized have a promising future in marine antifouling, and the strategy of combining multiple antifoulants can be a versatile orientation for developing environmentally friendly and efficient marine antifouling coatings.

**Author Contributions:** Data curation, D.W., R.L., X.L. (Xiaohui Liu), G.H. and Z.F.; formal analysis, X.L. (Xinrui Lin) and L.L.; writing—original draft, D.W. and M.D.; supervision, J.Y. and P.Z.; project administration, J.Y., J.C. and X.X.; funding acquisition, J.Y. All authors have read and agreed to the published version of the manuscript.

**Funding:** This research was funded by the Hainan Provincial Natural Science Foundation of China (Grant No. 221RC1016, No. 520MS015, No. 520MS040) and National Natural Science Foundation of China (Grant Nos. 52063011, 51663009).

**Institutional Review Board Statement:** Not applicable.

**Informed Consent Statement:** Not applicable.

**Data Availability Statement:** The data used to support the findings of this study are included within the article and are available from the corresponding author upon request.

**Conflicts of Interest:** The authors declare no conflict of interest.

## References

1. Prakash, S.; Ramasubburayan, R.; Iyapparaj, P.; Ramaswamy Arthi, A.P.; Ahila, N.K.; Ramkumar, V.S.; Immanuel, G.; Palavesam, A. Environmentally benign antifouling potentials of triterpene-glycosides from *Streptomyces fradiae*: A mangrove isolate. *RSC Adv.* **2015**, *5*, 29524–29534. [[CrossRef](#)]
2. Chen, Q.; Zhang, L.; Zhang, J.; Habib, S.; Lu, G.; Dai, J.; Liu, X. Bio-based polybenzoxazines coatings for efficient marine antifouling. *Prog. Org. Coat.* **2023**, *174*, 107298. [[CrossRef](#)]
3. Pourhashem, S.; Seif, A.; Saba, F.; Nezhad, E.G.; Ji, X.; Zhou, Z.; Zhai, X.; Mirzaee, M.; Duan, J.; Rashidi, A.; et al. Antifouling nanocomposite polymer coatings for marine applications: A review on experiments, mechanisms, and theoretical studies. *J. Mater. Sci. Technol.* **2022**, *118*, 73–113. [[CrossRef](#)]
4. Dai, G.; Xie, Q.; Ma, C.; Zhang, G. Biodegradable Poly(ester-co-acrylate) with Antifoulant Pendant Groups for Marine Anti-Biofouling. *ACS Appl. Mater. Interfaces* **2019**, *11*, 11947–11953. [[CrossRef](#)] [[PubMed](#)]
5. Xie, Q.; Pan, J.; Ma, C.; Zhang, G. Dynamic surface antifouling: Mechanism and systems. *Soft Matter* **2019**, *15*, 1087–1107. [[CrossRef](#)] [[PubMed](#)]
6. Sun, J.; Duan, J.; Liu, X.; Dong, X.; Zhang, Y.; Liu, C.; Hou, B. Environmentally benign smart self-healing silicone-based coating with dual antifouling and anti-corrosion properties. *Appl. Mater. Today* **2022**, *28*, 101551. [[CrossRef](#)]
7. Schultz, M.P.; Bendick, J.A.; Holm, E.R.; Hertel, W.M. Economic impact of biofouling on a naval surface ship. *Biofouling* **2011**, *27*, 87–98. [[CrossRef](#)]
8. Magin, C.M.; Cooper, S.P.; Brennan, A.B. Non-toxic antifouling strategies. *Mater. Today* **2010**, *13*, 36–44. [[CrossRef](#)]
9. Almeida, E.; Diamantino, T.C.; de Sousa, O. Marine paints: The particular case of antifouling paints. *Prog. Org. Coat.* **2007**, *59*, 2–20. [[CrossRef](#)]
10. Dong, M.; Liu, Z.; Gao, Y.; Wang, X.; Chen, J.; Yang, J. Synergistic effect of copolymeric resin grafted 1,2-benzisothiazol-3(2H)-one and heterocyclic groups as a marine antifouling coating. *RSC Adv.* **2021**, *11*, 18787–18796. [[CrossRef](#)]
11. Wang, X.; Dong, M.; Meng, Z.; Chen, J.; Yang, J.; Wang, X. Synthesis and Biological Activity of Acrylate Copolymers Containing 3-Oxo-N-allyl-1,2-benzisothiazole-3(2H)-carboxamide Monomer as a Marine Antifouling Coating. *ChemistryOpen* **2021**, *10*, 523–533. [[CrossRef](#)]
12. Callow, J.A.; Callow, M.E. Trends in the development of environmentally friendly fouling-resistant marine coatings. *Nat. Commun.* **2011**, *2*, 244. [[CrossRef](#)]
13. Jin, H.; Tian, L.; Bing, W.; Zhao, J.; Ren, L. Bioinspired marine antifouling coatings: Status, prospects, and future. *Prog. Mater. Sci.* **2022**, *124*, 100889. [[CrossRef](#)]
14. Selim, M.S.; El-Safty, S.A.; Shenashen, M.A.; Higazy, S.A.; Elmarakbi, A. Progress in biomimetic leverages for marine antifouling using nanocomposite coatings. *J. Mater. Chem. B* **2020**, *8*, 3701–3732. [[CrossRef](#)] [[PubMed](#)]
15. Labriere, C.; Elumalai, V.; Staffansson, J.; Cervin, G.; Le Norcy, T.; Denardou, H.; Rehel, K.; Moodie, L.W.K.; Hellio, C.; Pavia, H.; et al. Phidianidine A and Synthetic Analogues as Naturally Inspired Marine Antifoulants. *J. Nat. Prod.* **2020**, *83*, 3413–3423. [[CrossRef](#)] [[PubMed](#)]

16. Soliman, Y.A.A.; Brahim, A.M.; Moustafa, A.H.; Hamed, M.A.F. Antifouling evaluation of extracts from Red Sea soft corals against primary biofilm and biofouling. *Asian Pac. J. Trop. Biomed.* **2017**, *7*, 991–997. [[CrossRef](#)]
17. Melrose, J. Mucin-like glycopolymer gels in electrosensory tissues generate cues which direct electrolocation in amphibians and neuronal activation in mammals. *Neural Regen. Res.* **2019**, *14*, 1191–1195. [[CrossRef](#)] [[PubMed](#)]
18. Zhao, H.; Sun, Q.; Deng, X.; Cui, J. Earthworm-Inspired Rough Polymer Coatings with Self-Replenishing Lubrication for Adaptive Friction-Reduction and Antifouling Surfaces. *Adv. Mater.* **2018**, *30*, e1802141. [[CrossRef](#)] [[PubMed](#)]
19. Wang, P.; Zhang, D.; Lu, Z. Slippery liquid-infused porous surface bio-inspired by pitcher plant for marine anti-biofouling application. *Colloids Surf. B Biointerfaces* **2015**, *136*, 240–247. [[CrossRef](#)]
20. Bandyopadhyay, P.R.; Hellum, A.M. Modeling how shark and dolphin skin patterns control transitional wall-turbulence vorticity patterns using spatiotemporal phase reset mechanisms. *Sci. Rep.* **2014**, *4*, 6650. [[CrossRef](#)]
21. Zheng, L.; Sundaram, H.S.; Wei, Z.; Li, C.; Yuan, Z. Applications of zwitterionic polymers. *React. Funct. Polym.* **2017**, *118*, 51–61. [[CrossRef](#)]
22. Nurioglu, A.G.; Esteves, A.C.C.; de With, G. Non-toxic, non-biocide-release antifouling coatings based on molecular structure design for marine applications. *J. Mater. Chem. B* **2015**, *3*, 6547–6570. [[CrossRef](#)]
23. Takahashi, K. Release Rate of Biocides from Antifouling Paints. In *Ecotoxicology of Antifouling Biocides*; Springer: Tokyo, Japan, 2009; pp. 3–22.
24. Ding, W.; Ma, C.; Zhang, W.; Chiang, H.; Tam, C.; Xu, Y.; Zhang, G.; Qian, P.Y. Anti-biofilm effect of a butenolide/polymer coating and metatranscriptomic analyses. *Biofouling* **2018**, *34*, 111–122. [[CrossRef](#)] [[PubMed](#)]
25. Zhang, X.; Hao, X.; Qiu, S.; Lu, G.; Liu, W.; Wang, L.; Wei, Y.; Chen, B.; Lan, X.; Zhao, H. Efficient capture and release of carboxylatedbenzothiazolinone from UiO-66-NH<sub>2</sub> for antibacterial and antifouling applications. *J. Colloid. Interf. Sci.* **2022**, *623*, 710–722. [[CrossRef](#)]
26. Qian, P.Y.; Li, Z.; Xu, Y.; Li, Y.; Fusetani, N. Mini-review: Marine natural products and their synthetic analogs as antifouling compounds: 2009–2014. *Biofouling* **2015**, *31*, 101–122. [[CrossRef](#)] [[PubMed](#)]
27. Wang, C.-Y.; Wang, K.-L.; Qian, P.-Y.; Xu, Y.; Chen, M.; Zheng, J.-J.; Liu, M.; Shao, C.-L.; Wang, C.-Y. Antifouling phenyl ethers and other compounds from the invertebrates and their symbiotic fungi collected from the South China Sea. *AMB Express* **2016**, *6*, 102. [[CrossRef](#)]
28. Ge, H.; Liu, G.; Yin, R.; Sun, Z.; Chen, H.; Yu, L.; Su, P.; Sun, M.; Alamry, K.A.; Marwani, H.M.; et al. An aldimine condensation reaction based fluorescence enhancement probe for detection of gaseous formaldehyde. *Microchem. J.* **2020**, *156*, 104793. [[CrossRef](#)]
29. Wang, X.; Wang, X.; Dong, M.; Li, Z.; Liu, Z.; Lu, J.; Lin, Q.; Yang, J. Synthesis and biological activities of 1H-indole-1-carboxylic acid aryl esters as a marine antifouling coating. *J. Coat. Technol. Res.* **2020**, *17*, 553–561. [[CrossRef](#)]
30. Kabir, E.; Uzzaman, M. A review on biological and medicinal impact of heterocyclic compounds. *Results Chem.* **2022**, *4*, 100606. [[CrossRef](#)]
31. Saleh, S.S.; Al-Salihi, S.S.; Mohammed, I.A. Biological activity Study for some heterocyclic compounds and their impact on the gram positive and negative bacteria. *Energy Procedia* **2019**, *157*, 296–306. [[CrossRef](#)]
32. Moradi, M.; Duan, J.; Du, X. Investigation of the effect of 4,5-dichloro-2-n-octyl-4-isothiazolin-3-one inhibition on the corrosion of carbon steel in Bacillus sp. inoculated artificial seawater. *Corros. Sci.* **2013**, *69*, 338–345. [[CrossRef](#)]
33. Peng, K.; Dai, X.; Mao, H.; Zou, H.; Yang, Z.; Tu, W.; Hu, J. Development of direct contact-killing non-leaching antimicrobial polyurethanes through click chemistry. *J. Coat. Technol. Res.* **2018**, *15*, 1239–1250. [[CrossRef](#)]
34. Jo, Y.W.; Im, W.B.; Rhee, J.K.; Shim, M.J.; Kim, W.B.; Choi, E.C. Synthesis and antibacterial activity of oxazolidinones containing pyridine substituted with heteroaromatic ring. *Bioorg Med. Chem. Lett.* **2004**, *12*, 5909–5915. [[CrossRef](#)] [[PubMed](#)]
35. Gao, F.; Wang, T.; Xiao, J.; Huang, G. Antibacterial activity study of 1,2,4-triazole derivatives. *Eur. J. Med. Chem.* **2019**, *173*, 274–281. [[CrossRef](#)] [[PubMed](#)]
36. Eissa, S.I.; Farrag, A.M.; Abbas, S.Y.; El Shehry, M.F.; Ragab, A.; Fayed, E.A.; Ammar, Y.A. Novel structural hybrids of quinoline and thiazole moieties: Synthesis and evaluation of antibacterial and antifungal activities with molecular modeling studies. *Bioorg Chem.* **2021**, *110*, 104803. [[CrossRef](#)]
37. Ai, X.; Mei, L.; Ma, C.; Zhang, G. Degradable hyperbranched polymer with fouling resistance for antifouling coatings. *Prog. Org. Coat.* **2021**, *153*, 106141. [[CrossRef](#)]
38. Li, Y.; Chen, R.; Feng, Y.; Liu, L.; Sun, X.; Tang, L.; Takahashi, K.; Wang, J. Antifouling behavior of self-renewal acrylate boron polymers with pyridine-diphenylborane side chains. *New J. Chem.* **2018**, *42*, 19908–19916. [[CrossRef](#)]
39. Feng, K.; Ni, C.; Yu, L.; Zhou, W.; Li, X. Synthesis and evaluation of acrylate resins suspending indole derivative structure in the side chain for marine antifouling. *Colloid. Surf. B* **2019**, *184*, 110518. [[CrossRef](#)]
40. Zhou, W.; Wang, Y.; Ni, C.; Yu, L. Preparation and evaluation of natural rosin-based zinc resins for marine antifouling. *Prog. Org. Coat.* **2021**, *157*, 106270. [[CrossRef](#)]
41. Dong, R.; Wang, L.; Zhu, J.; Liu, L.; Qian, Y. A novel SiO<sub>2</sub>-GO/acrylic resin nanocomposite: Fabrication, characterization and properties. *Appl. Phys. A-Mater.* **2019**, *125*, 551. [[CrossRef](#)]
42. Yu, Z.; Yan, Z.; Zhang, F.; Wang, J.; Shao, Q.; Murugadoss, V.; Alhadhrani, A.; Mersal, G.A.M.; Ibrahim, M.M.; El-Bahy, Z.M.; et al. Waterborne acrylic resin co-modified by itaconic acid and  $\gamma$ -methacryloxypropyl triisopropoxidesilane for improved mechanical properties, thermal stability, and corrosion resistance. *Prog. Org. Coat.* **2022**, *168*, 106875. [[CrossRef](#)]

43. Cevik, P.; Yildirim-Bicer, A.Z. The Effect of Silica and Prepolymer Nanoparticles on the Mechanical Properties of Denture Base Acrylic Resin. *J. Prosthodont.* **2018**, *27*, 763–770. [[CrossRef](#)] [[PubMed](#)]
44. Dong, M.; Liu, L.; Wang, D.; Li, M.; Yang, J.; Chen, J. Synthesis and Properties of Self-Polishing Antifouling Coatings Based on BIT-Acrylate Resins. *Coatings* **2022**, *12*, 891. [[CrossRef](#)]
45. Passauer, L. A case study on the thermal degradation of an acrylate-type polyurethane wood coating using thermogravimetry coupled with evolved gas analysis. *Pro Org. Coat.* **2021**, *157*, 106331. [[CrossRef](#)]

**Disclaimer/Publisher's Note:** The statements, opinions and data contained in all publications are solely those of the individual author(s) and contributor(s) and not of MDPI and/or the editor(s). MDPI and/or the editor(s) disclaim responsibility for any injury to people or property resulting from any ideas, methods, instructions or products referred to in the content.